BIOCHEMISTRY
including biophysical chemistry & molecular biology

Article

pubs.acs.org/biochemistry

High-Risk Long QT Syndrome Mutations in the Kv7.1 (KCNQ1) Pore Disrupt the Molecular Basis for Rapid K^+ Permeation

Don E. Burgess,[†] Daniel C. Bartos,[†] Allison R. Reloj,[†] Kenneth S. Campbell,[†] Jonathan N. Johnson,[‡] David J. Tester,[‡] Michael J. Ackerman,[‡] Véronique Fressart,[§,∥] Isabelle Denjoy,[§,∥] Pascale Guicheney,[§,∥] Arthur J. Moss,[⊥] Seiko Ohno,[@] Minoru Horie,[@] and Brian P. Delisle*[,†]

[†]Center for Muscle Biology, Department of Physiology, University of Kentucky, 800 Rose Street, MS508, Lexington, Kentucky 40536, United States

[‡]Departments of Medicine, Pediatrics, and Molecular Pharmacology and Experimental Therapeutics/Divisions of Cardiovascular Diseases and Pediatric Cardiology, Mayo Clinic, Rochester, Minnesota 55905, United States

[§]INSERM, U956, Hôpital Pitié-Salpêtrière, Fondation ICAN, Paris, France

[∥]UPMC Univ Paris 06, UMR_S956, IFR14, Paris, France

[⊥]Department of Medicine, University of Rochester Medical Center, Rochester, New York 14642, United States

[@]Department of Cardiovascular and Respiratory Medicine, Shiga University of Medical Sciences, Seta-tsukinowa, Ohtsu 520-2192, Japan

Supporting Information

ABSTRACT: Type 1 long QT syndrome (LQT1) is caused by loss-of-function mutations in the *KCNQ1* gene, which encodes the K^+ channel (Kv7.1) that underlies the slowly activating delayed rectifier K^+ current in the heart. Intragenic risk stratification suggests LQT1 mutations that disrupt conserved amino acid residues in the pore are an independent risk factor for LQT1-related cardiac events. The purpose of this study is to determine possible molecular mechanisms that underlie the loss of function for these high-risk mutations. Extensive genotype−phenotype analyses of LQT1 patients showed that T322M-, T322A-, or G325R-Kv7.1 confers a high risk for LQT1-related cardiac events. Heterologous expression of these mutations with KCNE1 revealed they generated nonfunctional channels and caused dominant negative suppression of WT-Kv7.1 current. Molecular dynamics simulations of analogous mutations in KcsA (T85M-, T85A-, and G88R-KcsA) demonstrated that they disrupted the symmetrical distribution of the carbonyl oxygen atoms in the selectivity filter, which upset the balance between the strong attractive and K^+−K^+ repulsive forces required for rapid K^+ permeation. We conclude high-risk LQT1 mutations in the pore likely disrupt the architectural and physical properties of the K^+ channel selectivity filter.

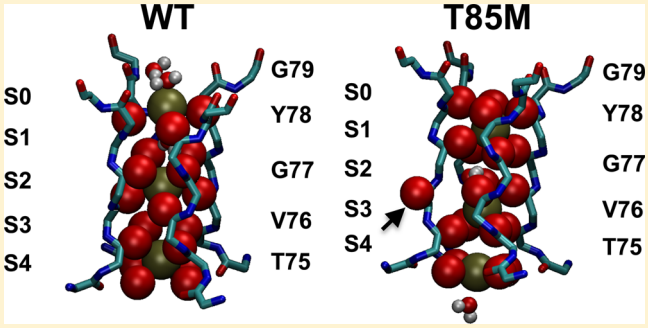

Congenital long QT syndrome (LQTS) is a monogenic cardiac arrhythmia syndrome that occurs in ∼1 in 2500 people and increases the risk for polymorphic ventricular tachycardia (torsades de pointes or torsades), syncope, and sudden death.[1−3] Type 1 long QT syndrome (LQT1) accounts for ∼35% of LQTS and is caused by loss-of-function mutations in the *KCNQ1* K^+ channel (Kv7.1).[4−12] Kv7.1 combines with the β-subunit KCNE1 to mediate the slowly activating delayed rectifier K^+ current in the heart (I_{Ks}). Intragenic risk stratification shows patients who have LQT1 missense mutations at conserved amino acids in the pore correlate with an increased risk for cardiac events (independent of QTc interval, gender, or β-blocker therapy).[13] The purpose of this study was to identify possible molecular mechanisms that underlie the loss of function for these high-risk LQT1 mutations.

The pore domain for all K^+ channels is composed of two transmembrane segments joined together by a linker that contains the conserved amino acids of the selectivity filter. X-ray analysis of a K^+ channel pore from *Streptomyces lividans* (KcsA) showed that the selectivity filter forms four contiguous K^+ binding sites (S1−S4).[14] On the basis of this structure, and molecular dynamics simulations (MDS) that calculate the energetics of permeation, the conduction of K^+ through the selectivity filter occurs by transitioning between two global states where two K^+ ions occupy S4 and S2, or S3 and S1.[15−21] The energetics for K^+ ions moving between these binding sites is essentially barrierless, but short-range K^+−K^+ repulsion

Received: July 16, 2012
Revised: October 23, 2012
Published: October 23, 2012

dx.doi.org/10.1021/bi3009449 | *Biochemistry* 2012, 51, 9076−9085

between the ions is essential for promoting the exit of the K^+ ion from S1 to a weak binding site outside the pore (S0).[15,19]

The KcsA selectivity filter is nearly identical to Kv7.1 (as well as most other K^+ selective channels). We made the simplifying assumption that the conserved amino acids in KcsA and Kv7.1 selectivity filters are structurally and functionally similar. This allowed us to study the impact of high-risk LQT1 pore mutations using the KcsA crystal structure. The advantage to using the KcsA structure is that it has been widely used to model K^+ ion permeation,[15−17,19,21,22] and similar to KCNE1-modified Kv7.1 channels, MDS show that the KcsA selectivity filter does not readily transit to nonconducting or inactivated states.[15,22]

EXPERIMENTAL PROCEDURES

Clinical. We identified more than 60 patients heterozygous for LQT1 missense mutations that disrupt a highly conserved threonine or glycine near the selectivity filter (T322M-, T322A-, or G325R-Kv7.1) (Table 1 and Table 1 of the Supporting Information).[23,24] One of these families (O) was reported previously.[25] Individual patient details are provided in Table 1 of the Supporting Information. The study was conducted according to the principles of the Helsinki Declaration. Blood samples were obtained after signed written informed consent for genetic analyses and after approval by the local institutional ethics committees. The respective protocols for research-based or commercially available genetic analyses of patients with LQTS were performed. Genomic DNA was isolated from blood leukocytes, and mutational analyses were performed using standard methods. The index patients in the families are negative for additional LQTS-associated mutations in both *KCNQ1* and the major LQTS susceptibility genes (except for the index patient in family A who has yet to be tested).

Table 1. Clinical Characteristics for Genotype Positive Patients with T322M-, T322A-, or G325R-Kv7.1[a]

no. of genotype positive families	26
no. with family history of symptoms	22
no. with T322M	13
no. with family history of symptoms	9
no. with T322A	2
no. with family history of symptoms	2
no. with G325R	11
no. with family history of symptoms	11
no. of genotype positive subjects (female, male)	63 (35, 28)
no. of symptomatic	29 (19, 10)
mean QTc ± SD (ms)	483 ± 44 (490 ± 32, 473 ± 55)
average age ± SD (years)	29 ± 18 (31 ± 20, 26 ± 17)
no. with T322M	29 (16, 13)
no. of symptomatic	12 (7, 5)
mean QTc ± SD (ms)	497 ± 43 (505 ± 32, 488 ± 54)
average age ± SD (years)	29 ± 18 (29 ± 20, 26 ± 16)
no. with T322A	12 (7, 5)
no. of symptomatic	2 (2, 0)
mean QTc ± SD (ms)	463 ± 27 (473 ± 22, 447 ± 27)
average age ± SD (years)	20 ± 16 (24 ± 18, 15 ± 12)
no. with G325R	22 (12, 10)
no. of symptomatic	15 (10, 5)
mean QTc ± SD (ms)	474 ± 47 (479 ± 31, 468 ± 63)
average age ± SD (years)	35 ± 19 (39 ± 20, 30 ± 18)

[a]Symptomatic is defined as experiencing syncope, torsades, or near drowning. See Table 1 of the Supporting Information for individual patient details.

Mutagenesis, Transfection, Electrophysiology, and Biotinylation. The appropriate nucleotide changes to generate the T322M-, T322A-, and G325R-Kv7.1 mutants were introduced into WT-Kv7.1 cDNA and used for electrophysiological studies in HEK293 cells as previously described.[26] To recapitulate I_{Ks}-like currents, all transfections included equal amounts of Kv7.1 and the auxiliary Kv7.1 β-subunit KCNE1 plasmid DNA (3 μg each). For coexpression studies, equal amounts of WT-Kv7.1 (1.5 μg) and mutant Kv7.1 (1.5 μg) were used to maintain the equivalent Kv7.1 plasmid DNA concentration (3 μg). The cells were cultured in MEM (with 10% fetal bovine serum) at 37 °C, and functional analyses were conducted using the standard whole-cell patch clamp technique 24−30 h after transfection. The external solution contained 137 mM NaCl, 4 mM KCl, 1.8 mM $CaCl_2$, 1 mM $MgCl_2$, 10 mM glucose, and 10 mM HEPES (pH 7.4 with NaOH), and an internal pipet solution contained 130 mM KCl, 1 mM $MgCl_2$, 5 mM EDTA, 5 mM MgATP, and 10 mM HEPES (pH 7.2 with KOH). An Axopatch-200B patch clamp amplifier (Axon Instruments, Union City, CA) was used to measure membrane currents and cell capacitance. Only cells with stable membrane resistances of >1 GΩ were studied. pCLAMP 10.0 (Axon Instruments) was used to generate the voltage clamp protocols, to acquire current signals, and to analyze data. Origin 7.0 (Microcal, Northhampton, MA) was used to perform Boltzmann fitting, to generate current−voltage (I−V) relations, and to plot graphs. The Boltzmann equation used to describe the I−V relations was

$$I = (I_{MIN} - I_{MAX})/[1 + e^{(V-V_{1/2})/k}] + I_{MAX}$$

where I_{MIN} is the minimally activated current, I_{MAX} is the maximally activated current, $V_{1/2}$ is the midpoint potential for half-maximal activation, and k is the slope factor (millivolts per e-fold change). For all experiments, the holding potential was −80 mV, and the dotted line in figures corresponds to the zero-current baseline. Voltage clamp experiments were performed at 22−23 °C within 1−2 h of the removal of cells from their culture conditions.

The biotinylation procedure was described previously.[26] Western blots of the biotinylated proteins were analyzed using the Odyssey infrared imaging system (Li-Cor, Lincoln, NE). The membranes were incubated in anti-Kv7.1 (Alomone laboratories, Jerusalem, Israel) and anti-Na^+/K^+-ATPase (Abcam, Cambridge, MA) to normalize for the biotinylation reaction. The appropriate IRdye secondary antibodies (Li-Cor) were used to detect anti-Kv7.1 and anti-Na^+/K^+-ATPase. To ensure that the cell surface biotinylation did not label intracellular proteins, the samples were probed with anti-calnexin (Abcam). Odyssey (Li-Cor) was used to quantify the density of the protein bands. The relative intensity of Kv7.1 to Na^+/K^+-ATPase intensity was calculated by normalizing the intensity of the Kv7.1 signal to the intensity of the Na^+/K^+-ATPase signal.

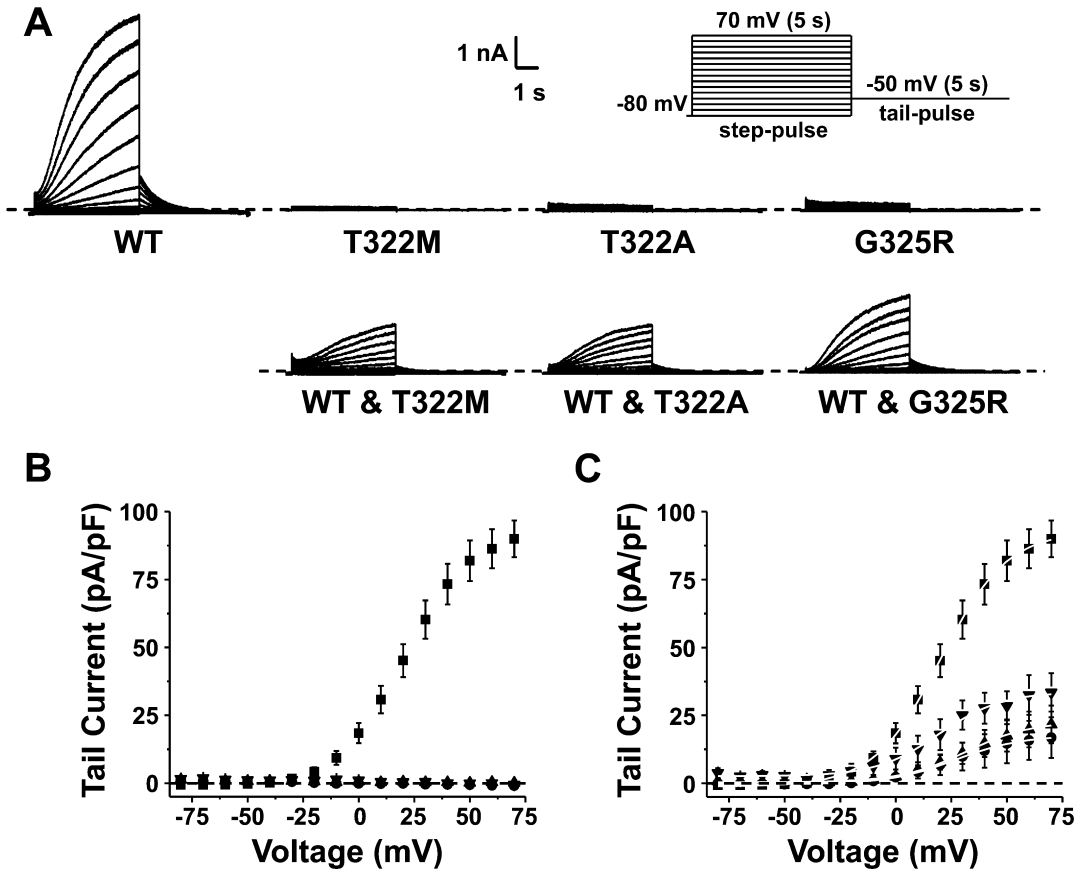

Figure 1. T322M-, T322A-, and G325R-Kv7.1 generate nonfunctional channels and cause dominant negative suppression of WT-Kv7.1 current. (A) Representative families of currents recorded from cells expressing WT-, T322M-, T322A-, or G325R-Kv7.1 using the voltage protocol shown. Also shown are representative families of currents from cells coexpressing WT- and T322M-, T322A-, or G325R-Kv7.1. (B) The graph shows the corresponding mean *I*–*V* relations for the peak tail current plotted as a function of the test voltage for WT-Kv7.1 (black filled squares), T322M-Kv7.1 (gray filled circles), T322A-Kv7.1 (gray upward-pointing triangles), or G325R-Kv7.1 (gray downward-pointing triangles). (C) The graph shows the corresponding mean *I*–*V* relations for the peak tail current plotted as a function of the test voltage for WT-Kv7.1 (black filled squares), WT- and T322M-Kv7.1 (gray filled circles), WT- and T322A-Kv7.1 (gray upward-pointing triangles), or WT- and G325R-Kv7.1 (gray downward-pointing triangles). The mean peak *I*–*V* relations were described using a Boltzmann equation (gray line). All of these studies included KCNE1.

Molecular Dynamics Simulations. Details regarding the MDS are provided in the Supporting Information. Briefly, the MDS systems for the KcsA channels (Protein Data Bank entry 1k4c)[27] were constructed using Visual Molecular Dynamics (VMD),[28] and KcsA simulations were performed using NAMD (Not just Another Molecular Dynamics program).[29] The KcsA structure was used to generate a channel embedded in a lipid bilayer consisting of 1-palmitoyl-2-palmitoleoyl-*sn*-glycero-3-phosphocholine (POPC) molecules, with explicit water, K^+ ions, and Cl^- ions. Two K^+ ions were placed in the selectivity filter, and one was placed in the cavity. A series of short MDS were performed to equilibrate the system as a whole. Production simulations were performed for up to 60 ns. A time step of 2 fs was employed in all simulations, and the atomic trajectory data were written at 1 ps intervals. VMD was used to analyze the atomic trajectories. MDS showed that the root-mean-square deviation (rmsd) values for α-carbon (C_α) backbone and amino acids quickly reached steady state after 5 ns. The relative rmsd values for the WT and mutant simulations were similar to one another (data not shown), suggesting that the mutations did not grossly affect channel stability.

Statistical Analysis. Data are reported as the mean ± the standard error (SE) unless otherwise noted. A one-way analysis of variance with a Bonferroni post hoc test was used to determine if either of the mutant parameters differed from that of WT ($p < 0.05$ was considered significant).

RESULTS

The purpose of this study is to identify the possible molecular mechanisms for high-risk LQT1 mutations in the pore domain. Because of the wide range of LQT1 expressivity in patients, a large number of patients with the same mutation need to be studied to confirm that they confer a high risk for LQT1-related cardiac events. We identified more than 60 patients from 26 families that are heterozygous for LQT1 mutations T322M-, T322A-, and G325R-Kv7.1 (Figure 1, Table 1, and Table 1 of the Supporting Information).[11] More than one-third of the patients have marked QT prolongation (QTc ≥ 500 ms), and ~85% of these families have histories of syncope, torsades, near drowning, or sudden cardiac death triggered primarily by exercise or swimming.[30] Overall, the clinical data from this large cohort suggested that T322M-, T322A-, and G325R-Kv7.1 confer a high risk for LQT1-related events.

dx.doi.org/10.1021/bi3009449 | *Biochemistry* 2012, 51, 9076–9085

We studied the functional phenotypes for these mutations by voltage-clamping cells transiently expressing WT-, T322M-, T322A-, or G325R-Kv7.1 with KCNE1 (Figure 1A). Macroscopic currents were recorded by applying steplike pulses from −80 to 70 mV in 10 mV increments for 5 s, followed by a "tail" pulse for 5 s to −50 mV (Figure 1A). The peak current amplitude recorded at the start of the tail pulse was plotted as a function of the step pulse potential for cells expressing WT-, T322M-, T322A-, or G325R-Kv7.1 (Figure 1B). To mimic the patients' heterozygous genotype, we also studied cells coexpressing WT- and T322M-, T322A-, or G325R-Kv7.1 (Figure 1A,C). Cells expressing WT-Kv7.1 generated large currents that resembled native I_{Ks}; cells expressing T322M-, T322A-, or G325R-Kv7.1 did not generate current, and cells coexpressing WT- and T322M-Kv7.1, T322A-Kv7.1, or G325R-Kv7.1 conducted only small currents (Figure 1B). The $I-V$ relations for the peak tail current were plotted as a function of the step voltage, and the data were described with a Boltzmann function to calculate changes in I_{MAX}, $V_{1/2}$, and k. Cells coexpressing WT- and T322M-Kv7.1, T322A-Kv7.1, or G325R-Kv7.1 reduced the I_{MAX} by ~70% with only small changes in activation gating (Table 2 of the Supporting Information). Importantly, the loss-of-function phenotype was not linked to coexpression of KCNE1, because cells expressing WT-, T322M-, T322A-, or G325R-Kv7.1 without KCNE1 showed that the mutations still did not generate any current (data not shown). These data demonstrate that T322M-, T322A-, and G325R-Kv7.1 caused a complete loss of Kv7.1 current and dominant negative suppression of WT-Kv7.1 current.

We tested whether T322M-, T322A-, and G325R-Kv7.1 caused a loss of function by simply reducing the amount of Kv7.1 expressed at the cell surface membrane. Biotinylation assays showed that cells expressing T322M-, T322A-, or G325R-Kv7.1 and KCNE1 reduced the level of cell surface membrane expression of Kv7.1 (Figure 1A,C of the Supporting Information). However, the reduction was insufficient to explain a complete loss of current (Figure 1A,B). Additionally, although cells coexpressing WT-Kv7.1 and T322M-, T322A-, or G325R-Kv7.1 showed dominant negative functional effects (Figure 1A,C), they did not show a decrease in the level of Kv7.1 at the cell surface membrane (Figure 1B,C of the Supporting Information). Together, these data suggest that a decrease in the level of Kv7.1 expression at the cell surface membrane does not account for the mutations' complete loss-of-function or dominant negative phenotypes.

The mutated threonine and glycine are highly conserved pore residues in the K^+ channel family (Figure 2A). Given their proximity to the K^+ channel selectivity filter (Figure 2B), we tested whether incorporating analogous mutations into the KcsA structure altered the architecture of the selectivity filter and permeation events. Panels C−F of Figure 2 show representative MDS images for the WT-, T85M-, T85A-, and G88R-KcsA selectivity filters, respectively. The WT-KcsA selectivity filter formed four contiguous sites that could bind to K^+ ions and water molecules in an alternating manner. For the most part, the oxygen atoms that lined the WT-KcsA selectivity filter faced the central pore axis; however, similar to what has been shown by others,[17,21,22] the carbonyl oxygen atom between S2 and S3 (V76) on each α-subunit could briefly "flip" away from the central pore axis (Movie 1 of the Supporting Information). The representative selectivity filter images for the T85M-, T85A-, and G88R-KcsA simulations

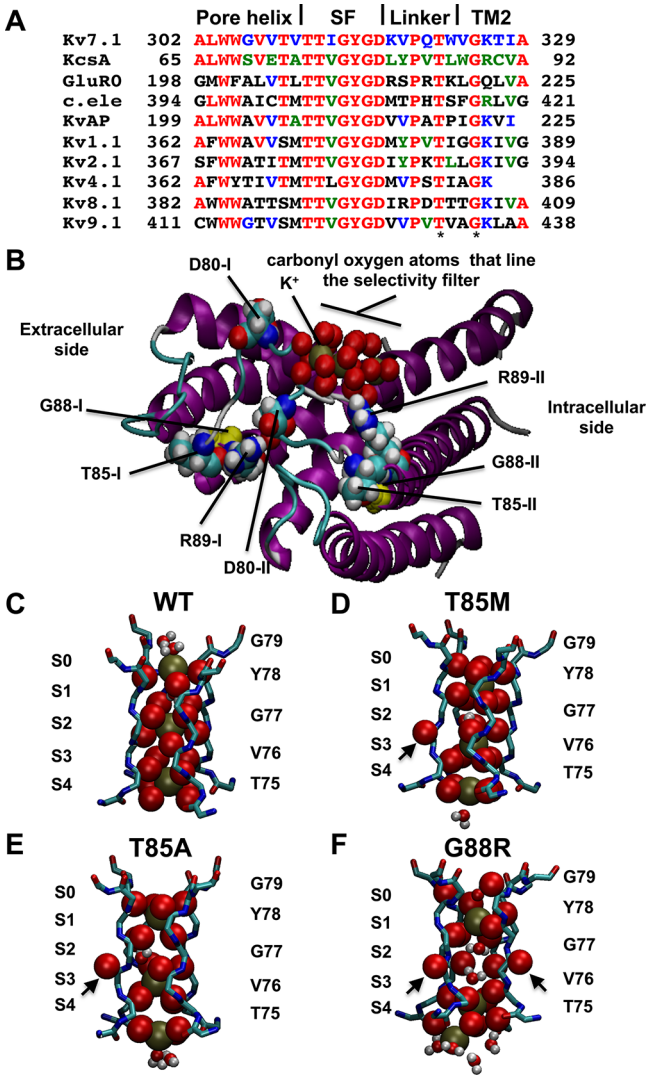

Figure 2. Sequence alignment of the K^+ channel pore domain and the position of the conserved threonine and glycine with respect to the K^+ channel selectivity filter. (A) Sequence alignments of the selectivity filter for different K^+ channels: Kv7.1 (GenBank entry NP_000208NP_000209); KcsA (GenBank entry NP_000208NP_631700.1); GluR0, ionotropic glutamate receptor from *Nostoc punctiforme* (Swiss-Prot entry P73797); c. ele, voltage-dependent K^+ channel from *Caenorhabditis elegans* (GenBank entry AAB95119.1); KvAP, voltage-dependent K^+ channel from *Aeropyrum pernix* (Swiss-Prot entry Q9YDF8.1); Kv1.1 (GenBank entry NP_000208); Kv2.1 (GenBank entry AAB88808.1); Kv4.1 (GenBank entry NP_004970.3); Kv8.1 (GenBank entry NP_055194.1); Kv9.1 (GenBank entry NP_002242.2). Only amino acid residues that correspond to the pore helix, the selectivity filter (SF), and the linker between the selectivity filter and the second transmembrane segment (TM2) in the pore domain are shown. The asterisks denote the conserved threonine and glycine disrupted by T322M-, T322A-, and G325R-Kv7.1 mutations. Red residues are conserved in Kv7.1 and KcsA. Blue residues are conserved in Kv7.1 but not KcsA. Green residues are conserved in KcsA but not Kv7.1. Black residues are not conserved in Kv7.1 or KcsA. (B) Ribbon structure of two adjacent KcsA α-subunits (I and II) (purple) with the space filled van der Waal spheres for the conserved threonine (T85) and glycine (G88) (light blue for C, red for O, dark blue for N, and gray for H; the glycine atoms are all colored yellow for the sake of clarity). Also shown are the van der Waals spheres for the conserved aspartate in the K^+ channel selectivity filter (D80), conserved arginine/lysine (R89), the carbonyl oxygen atoms that line the selectivity filter from all four α-subunits,

dx.doi.org/10.1021/bi3009449 | *Biochemistry* 2012, 51, 9076−9085

Figure 2. continued

and the K^+ ions (green) in the selectivity filter. The threonine and glycine are in the proximity of the aspartate in the selectivity filter of the adjacent subunit. (C–F) Representative atomic-scale image of the selectivity filter for (C) WT-, (D) T85M-, (E) T85A-, or (F) G88R-KcsA MDS. Shown are the main chain backbones for selectivity filter residues TVGYG (light blue for C, red for O, and dark blue for N) for all four α-subunits, the bound K^+ ions (green), and several adjacent water molecules (red for O and gray for H). The oxygen atoms that line the filter and the K^+ ions are shown as large spheres, and water molecules are shown as small spheres for emphasis. S0–S4 approximate the different binding sites. The arrows highlight the α-subunits in the flipped configuration.

showed that these mutations essentially stabilized the flipped configuration (Figure 2D–F and Movies 2–4 of the Supporting Information). T85M- and T85A-KcsA stabilized the flipped configuration for one of the α-subunits (Figure 2D,E), and G88R-KcsA stabilized the flipped configuration for two adjacent α-subunits (Figure 2F). The transition of the flipped carbonyl oxygen away from the central pore axis reflects a change in the dihedral angles around the V76–G77 amide plane. This can be visualized in an overlay of Ramachandran plots calculated at each picosecond of the simulation for the four α-subunits. Figure 3A shows the overlay of the Ramachandran plots for the WT-KcsA α-subunits. The dihedral angles for V76 and G77 are the most dynamic, which reflects the carbonyl oxygen alternating between the central pore axis

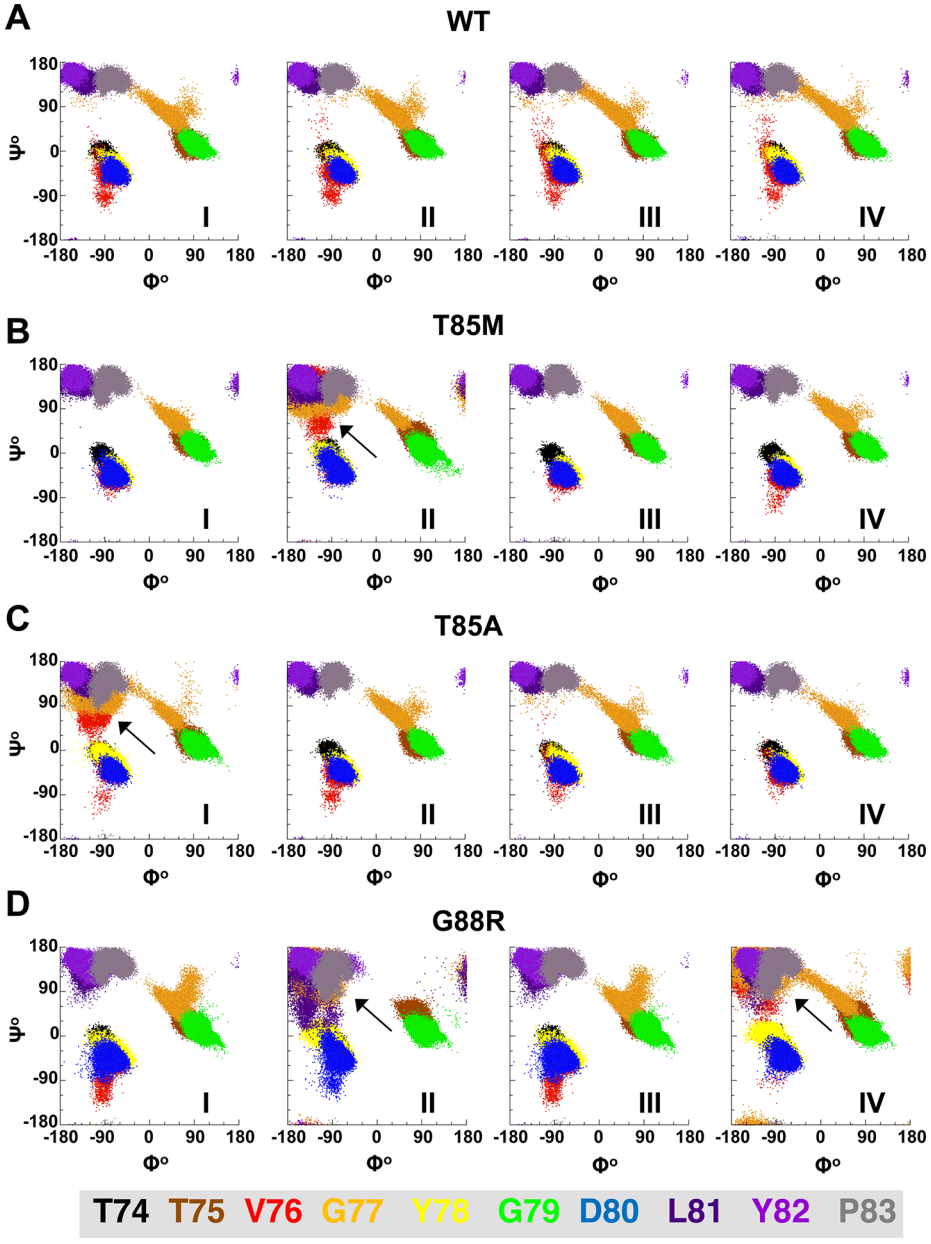

Figure 3. T85M-, T85A-, G88R-KcsA α-subunits in the flipped configuration disrupt the bond angle symmetry for the amino acid residues in the selectivity filter. An overlay of Ramachandran plots calculated at each picosecond from the trajectory file for the different selectivity filter amino acid residues (black for T74, brown for T75, red for V76, orange for G77, yellow for Y78, green for G79, blue for D80, violet for L81, purple for Y, and gray for P83) for (A) WT-, (B) T85M-, (C) T85A-, or (D) G88R-KcsA α-subunits (I–IV). The arrows highlight the Ramachandran plots for the mutant α-subunits that have a stable flipped configuration.

dx.doi.org/10.1021/bi3009449 | *Biochemistry* 2012, 51, 9076–9085

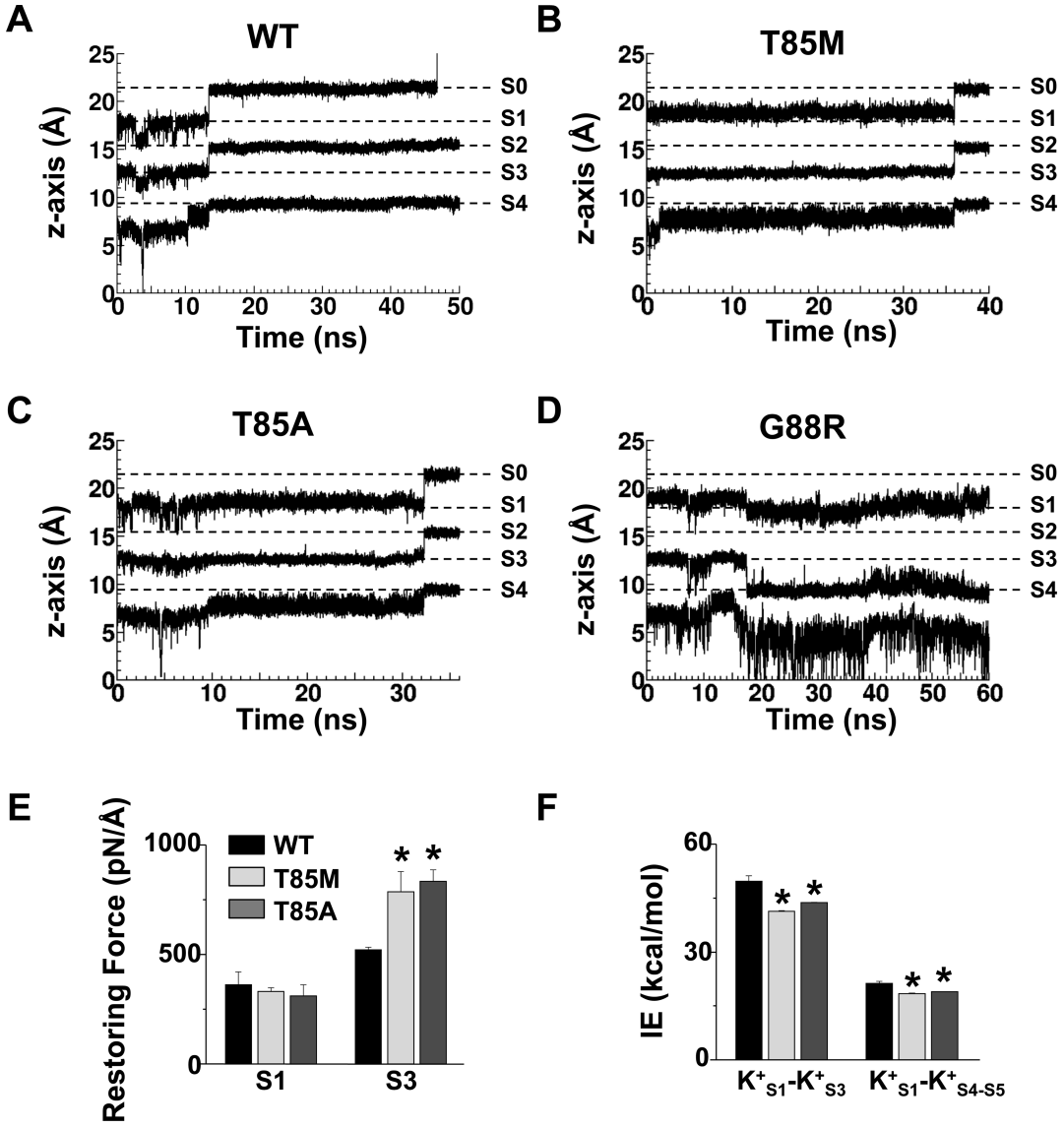

Figure 4. T85M-, T85A-, and G88R-KcsA mutations delay or disrupt the K^+ permeation step, and T85M- and T85A-KcsA mutations increase the K^+ restoring force at S3 and weaken K^+–K^+ repulsion at S1. (A–D) The graphs show the movement of the three K^+ ions for (A) WT-, (B) T85M-, (C) T85A-, or (D) G88R-KcsA simulations along the *z*-axis over time. The origin for the *z*-coordinate is the center of the membrane (0 Å), and S0–S4 approximate the different binding sites from the WT-KcsA simulation. (E) The graph shows the mean restoring force calculated at S1 and S3 for WT-KcsA (black), T85M-KcsA (light gray), or T85A-KcsA (dark gray) (n = 3 simulations each) (*p < 0.05 compared to control). (F) The graph shows the mean interaction energies between the different K^+ ions at S1 (K^+_{S1}) or S3 (K^+_{S3}) or the K^+ ion moving into S4 (K^+_{S4-S5}) for WT-KcsA (black), T85M-KcsA (light gray), or T85A-KcsA (dark gray) (n = 3 simulations each) (*p < 0.05 compared to control).

and flipped configuration. The Ramachandran plots for each WT-KcsA α-subunit are similar or symmetrical to one another. Panels B–D of Figure 3 show the Ramachandran plots for T85M-, T85A-, and G88R-KcsA, respectively. Notice the mutant α-subunits that stabilize the flipped configuration have very different Ramachandran plots when compared to the other α-subunits.

All the simulations were initiated with K^+ ions at a weak binding site in the cavity (S5) and at S3–S1. The WT-KcsA simulation showed that the three K^+ ions had moved from the initial (S5)–S3–S1 state to an S4–S2–(S0) state (Figure 2C). On the basis of the relative location of the K^+ ions in the images from the mutant MDS (Figure 2D–F), the α-subunit(s) in the flipped configuration delayed the K^+ ions from moving into the S4–S2–(S0) state. To better appreciate the dynamic movement of the different K^+ ions during the simulations, we plotted their *z*-axis coordinates over time (Figure 4). The WT-KcsA simulation showed that the K^+ ion at S5 quickly approached S4, which was accompanied by the coordinated movement of the three K^+ ions to the S4–S2–(S0) state (Figure 4A). This permeation step is qualitatively similar to the knock-on mechanism originally proposed by Hodgkin and Keynes[31] and described in detail by Berneche and Roux for KcsA.[15] The T85M- and T85A-KcsA simulations showed a similar permeation step but with a much longer delay (Figure 4B,C). Closer examination of the T85M- and T85A-KcsA simulations showed that the permeation could not occur as long as one of the α-subunits was in the flipped configuration. In contrast, the G88R-KcsA simulation showed dramatically different K^+ ion trajectories (Figure 4D). The K^+ ion at S5 approached S4 but then moved back into the cavity; the K^+ ion at S3 then moved to S4, and the K^+ ion at S1 stayed in place.

dx.doi.org/10.1021/bi3009449 | *Biochemistry* 2012, 51, 9076–9085

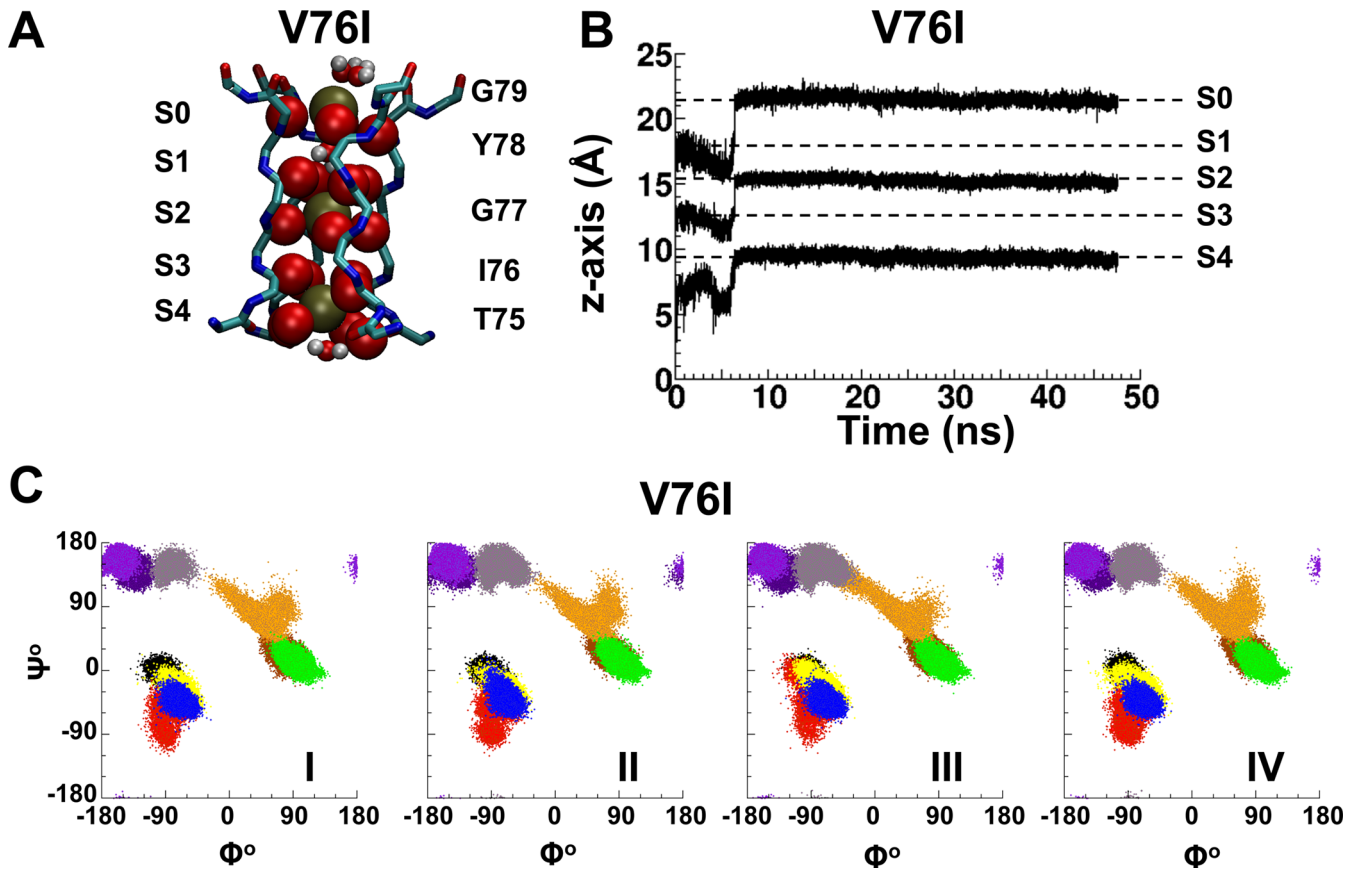

Figure 5. V76I-KcsA substitution that does not disrupt the binding sites in the selectivity filter or K^+ permeation. (A) Representative atomic image of the selectivity filter for V76I-KcsA. Shown are the TIGYG amino acid residues (light blue for C, red for O, and dark blue for N) for all four α-subunits, the bound K^+ ions (green), and several adjacent water molecules (red for O and gray for H). The oxygen atoms that line the filter and the K^+ ions are shown as large spheres, and water molecules are shown as small spheres for emphasis. S0−S4 approximate the different binding sites. (B) The graphs show the movement of the three K^+ ions along the z-axis over time. The origin for the z-coordinate axis is the center of the membrane, and S0−S4 approximate the different binding sites from the WT-KcsA simulation. V76I-KcsA does not delay or disrupt the permeation step. (C) Cumulative Ramachandran plots for the different selectivity filter amino acid residues (black for T74, brown for T75, red for I76, orange for G77, yellow for Y78, green for G79, blue for D80, violet for L81, purple for Y, and gray for P83) calculated for the four (I−IV) V76I-KcsA α-subunits. The Ramachandran plots for each V76I-KcsA α-subunit are similar to one another and to that of the WT-KcsA α-subunits (Figure 3A).

Because T85M- or T85A-KcsA delayed (but did not prevent) the permeation step, we speculated that they alter the relative attractive−repulsive forces that underlie rapid K^+ permeation. Accordingly, we calculated the change in the K^+ ion restoring force at S3 and the interaction energy (mainly Columbic repulsion) between the different K^+ ions (Figure 4E,F). When one of the α-subunits was in the flipped configuration, the K^+ ion at S3 interacted more closely with the remaining carbonyl oxygen atoms and the net electrostatic repulsion with the K^+ ion at S1 was decreased. Together, the data suggest that T85M- or T85A-KcsA upsets the balance of forces needed to facilitate that rapid exit of the K^+ ion at S1.

To ensure the robustness of the MDS, we performed a negative control by testing a substitution in the KcsA selectivity filter that is not expected to negatively affect K^+ permeation. V76 in the KcsA selectivity filter corresponds to I313 in the Kv7.1 (Figure 2A). This is a very conservative substitution whose side chain differs by only one methylene group, and functional studies show that the engineered I313V-Kv7.1 mutant is not different when compared to WT-Kv7.1.[32] MDS of V76I-KcsA demonstrated it behaved like WT-KcsA (Figure 5A−C).

DISCUSSION

A major challenge for clinicians is to determine which therapeutic strategy is the most appropriate for an individual LQT1 patient. The value of genetic testing in selecting the proper therapy for a given patient is limited because of its inability to predict functional phenotypes accurately or forecast disease expressivity and/or severity. In an effort to move beyond genotype risk stratification simply based on the type of LQTS (i.e., LQT1, LQT2, LQT3, etc.), multiple studies are identifying intragenic approaches to correlate the risk for LQT-related cardiac events based on the type, location, and dysfunction of a mutation.[9,13,33−35] These types of studies found that LQT1 mutations that disrupt conserved amino acids in the pore region are an independent risk factor for cardiac events.[13] The purpose of this work was to provide molecular insight into how these high-risk LQT1 mutations might cause channels to malfunction. We were able to generate a robust molecular model for high-risk LQT1 mutations by (1) identifying a number of different LQT1 patients with the same mutations in the pore, (2) studying their functional phenotypes in vitro, and (3) performing MDS of analogous mutations in KcsA. The clinical data confirmed that these mutations conferred a high risk for LQT1-related events, and

dx.doi.org/10.1021/bi3009449 | Biochemistry 2012, 51, 9076−9085

the in vitro data suggested that mutations generate nonfunctional Kv7.1 channels and dominant negative effects. The in silico data suggested a mechanism for the disruption of channel function, namely, that a backbone conformational change disrupts permeation through the selectivity filter.

A major advantage in studying the LQT1 mutations using KcsA is that an effective model for K^+ permeation has been developed for this structure.[15] MDS that calculated the energetics of KcsA permeation suggest that the movement of K^+ ions between binding sites in the selectivity filter is essentially barrierless; however, the K^+ ion at S1 is in a deep energy well and cannot exit toward S0.[15,19] Berneche and Roux proposed that this is overcome by electrostatic repulsion between the other K^+ ions in the pore. As the K^+ ion at S5 approaches S4, the second K^+ ion at S3 initiates its transition to S2, and electrostatic repulsion from the incoming K^+ ion at S4 and the K^+ ion transiting to S2 lift the bottom of the deep free energy well for the K^+ ion at S1. Ultimately, the K^+ ion at S1 becomes unstable and exits toward S0. Without the repulsion from the other two incoming ions, the K^+ ion at S1 remains trapped in its deep energy well.

The K^+ trajectories for our WT-KcsA MDS are in good agreement with this energetic model of K^+ permeation (Figure 4A). We found that incorporating T85M- and T85A-KcsA mutations primarily altered the S2−S3 binding site and decreased the net electrostatic repulsion from the incoming K^+ ion at S4 and the ion at S3 (Figure 4F). The simulations suggested that this would increase the level of trapping of the K^+ ion at S1 (Figure 4B,C) and decrease the level of K^+ permeation. The effect that G88R-KcsA had on the S2−S3 binding site was much more severe and appeared to prevent the permeation step altogether.

The modeling raises several questions, including how different mutations stabilize the flipped configuration and why this is seen for one or more of the α-subunits. The simulations showed that T85M-, T85A-, and G88R-KcsA similarly potentiated the formation of hydrogen bonds between D80 and the R89 residue on the adjacent α-subunit (Figure 2B). We speculate the potentiation of this bond might increase the stability of the flipped configuration. The simulations also showed that when one of the T85M- or T85A-KcsA α-subunits entered the flipped configuration, the K^+ ion at S3 more closely associated with the remaining carbonyl oxygen atoms (Figure 44E, movies 2,3 of the Supporting Information). This likely prevented the remaining α-subunits from entering the flipped configuration. However, if the K^+ ion binding to S3 is lost, as it was in the G88R-KcsA simulation, then we suspect that all four of the α-subunits would eventually enter the flipped configuration. Indeed, not only a second but a third G88R-KcsA α-subunit entered the flipped configuration after 55 ns (data not shown).

There are several limitations to our approach. The functional data were obtained in a widely used heterologous expression system and may not completely recapitulate the native condition. Although the availability of a high-quality structure for the closely related KcsA allowed us to investigate the molecular basis for the functional disruption by the different LQT1 mutations, not all of the KcsA pore residues are identical to Kv7.1. To circumvent this, we attempted to perform MDS using a published Kv7.1 homology model. However, this proved to be problematic because the selectivity filter was unstable and required the application of dihedral restraints to support permeation (data not shown).[36] A more recent Kv7.1 homology model also proved to be problematic because the selectivity filter is in a C-type inactivated configuration.[37] A second limitation to using KcsA is that it does not include the obligatory I_{Ks} β-subunit KCNE1. KCNE1 profoundly affects Kv7.1 by eliminating C-type inactivation.[38−41] Studies suggest that KCNE1 eliminates C-type inactivation by interacting with a phenylalanine (F340) in the second transmembrane segment of the pore domain, near the hinge region responsible for opening the channel. This phenylalanine is conserved in KcsA (F103),[42] and studies indicate that, as KcsA opens, F103 reorients to form a hydrogen bond network in the selectivity filter to facilitate C-type inactivation.[43,44] The interplay between KcsA opening and C-type inactivation is expected to occur in other K^+ channels, including Kv7.1.[42−44] Assuming KCNE1 prevents the reorientation of F340 in Kv7.1 to eliminate C-type inactivation, then the closed KcsA structure (which has F103 in an orientation that does not promote C-type inactivation) might represent an adequate surrogate to model the selectivity filter of a KCNE1-modified Kv7.1 channel. Lastly, MDS using KcsA do not provide mechanistic insight into how the mutations alter the cell surface membrane expression of Kv7.1 or its voltage-dependent gating. On the basis of the functional data, these changes do not likely account for the high-risk phenotypes in the patients. The level of cell surface expression of Kv7.1 was not decreased under conditions that mimicked heterozygosity (Figure 1B of the Supporting Information), and there are only relatively weak effects on gating (Table 2 of the Supporting Information).

In summary, we identified atomic-scale changes associated with higher-risk, dominant negative, pore-localizing LQT1-causative mutations. These data support the notion that MDS may assist in the pathogenic assessment of high-risk LQT1 mutations. We expect that subsequent advances in crystallography and homology modeling and improvements in the force field and computer hardware for MDS will further the applicability of this approach to nonconserved residues, other regions of Kv7.1, and other processes disrupted by LQT1 mutations (i.e., gating, co-assembly, phosphorylation, etc.).

■ ASSOCIATED CONTENT

Supporting Information

Supplemental experimental procedures, Figure 1, Movies 1−4, and Tables 1 and 2. This material is available free of charge via the Internet at http://pubs.acs.org.

■ AUTHOR INFORMATION

Corresponding Author

*Address: 800 Rose St., MS508, Lexington, KY 40536. Telephone: (859) 323-2797. Fax: (859) 323-1070. E-mail: brian.delisle@uky.edu.

Funding

This work was supported by American Heart Association Predoctoral Award PRE7370003 (D.C.B.) and National Heart, Lung and Blood Institute Grant R01 HL087039 (B.P.D.).

Notes

We declare the following competing financial interest(s): Dr. Michael J. Ackerman is a consultant for Biotronik, Boston Scientific, Medtronic, St. Jude Medical, and Transgenomic. In addition, there is a license agreement held between Transgenomic and Mayo Clinic Health Solutions, and royalties are distributed in accordance with Mayo Clinic policy.

■ ACKNOWLEDGMENTS

We acknowledge Dr. David Rodgers (University of Kentucky) for critical review of the manuscript, Eric S. Schmidt, McKenzie Johnson, and Jennifer L. Smith (University of Kentucky) for their technical assistance, and the University of Kentucky Information Technology department and Center for Computational Sciences for computing time on the Lipscomb High Performance Computing Cluster.

■ ABBREVIATIONS

LQTS, long QT syndrome; LQT1, type 1 long QT syndrome; MDS, molecular dynamics simulations; VMD, Visual Molecular Dynamics; NAMD, Not Just Another Molecular Dynamics program; POPC, palmitoyl-2-palmitoleoyl-*sn*-glycero-3-phosphocholine; rmsd, root-mean-square deviation.

■ REFERENCES

(1) Ward, O. C. (1964) A New Familial Cardiac Syndrome in Children. *J. Ir. Med. Assoc. 54*, 103−106.

(2) Romano, C. (1965) Congenital Cardiac Arrhythmia. *Lancet 1*, 658−659.

(3) Lehnart, S. E., Ackerman, M. J., Benson, D. W., Jr., Brugada, R., Clancy, C. E., Donahue, J. K., George, A. L., Jr., Grant, A. O., Groft, S. C., January, C. T., Lathrop, D. A., Lederer, W. J., Makielski, J. C., Mohler, P. J., Moss, A., Nerbonne, J. M., Olson, T. M., Przywara, D. A., Towbin, J. A., Wang, L. H., and Marks, A. R. (2007) Inherited arrhythmias: A National Heart, Lung, and Blood Institute and Office of Rare Diseases workshop consensus report about the diagnosis, phenotyping, molecular mechanisms, and therapeutic approaches for primary cardiomyopathies of gene mutations affecting ion channel function. *Circulation 116*, 2325−2345.

(4) Kapplinger, J. D., Tester, D. J., Salisbury, B. A., Carr, J. L., Harris-Kerr, C., Pollevick, G. D., Wilde, A. A., and Ackerman, M. J. (2009) Spectrum and prevalence of mutations from the first 2,500 consecutive unrelated patients referred for the FAMILION long QT syndrome genetic test. *Heart Rhythm 6*, 1297−1303.

(5) Wang, Q., Curran, M. E., Splawski, I., Burn, T. C., Millholland, J. M., VanRaay, T. J., Shen, J., Timothy, K. W., Vincent, G. M., de Jager, T., Schwartz, P. J., Toubin, J. A., Moss, A. J., Atkinson, D. L., Landes, G. M., Connors, T. D., and Keating, M. T. (1996) Positional cloning of a novel potassium channel gene: KVLQT1 mutations cause cardiac arrhythmias. *Nat. Genet. 12*, 17−23.

(6) Chouabe, C., Neyroud, N., Guicheney, P., Lazdunski, M., Romey, G., and Barhanin, J. (1997) Properties of KvLQT1 K^+ channel mutations in Romano-Ward and Jervell and Lange-Nielsen inherited cardiac arrhythmias. *EMBO J. 16*, 5472−5479.

(7) Wollnik, B., Schroeder, B. C., Kubisch, C., Esperer, H. D., Wieacker, P., and Jentsch, T. J. (1997) Pathophysiological mechanisms of dominant and recessive KVLQT1 K^+ channel mutations found in inherited cardiac arrhythmias. *Hum. Mol. Genet. 6*, 1943−1949.

(8) Neyroud, N., Denjoy, I., Donger, C., Gary, F., Villain, E., Leenhardt, A., Benali, K., Schwartz, K., Coumel, P., and Guicheney, P. (1998) Heterozygous mutation in the pore of potassium channel gene KvLQT1 causes an apparently normal phenotype in long QT syndrome. *Eur. J. Hum. Genet. 6*, 129−133.

(9) Chouabe, C., Neyroud, N., Richard, P., Denjoy, I., Hainque, B., Romey, G., Drici, M. D., Guicheney, P., and Barhanin, J. (2000) Novel mutations in KvLQT1 that affect Iks activation through interactions with Isk. *Cardiovasc. Res. 45*, 971−980.

(10) Deschenes, D., Acharfi, S., Pouliot, V., Hegele, R., Krahn, A., Daleau, P., and Chahine, M. (2003) Biophysical characteristics of a new mutation on the KCNQ1 potassium channel (L251P) causing long QT syndrome. *Can. J. Physiol. Pharmacol. 81*, 129−134.

(11) Ruan, Y., Liu, N., Napolitano, C., and Priori, S. G. (2008) Therapeutic strategies for long-QT syndrome: Does the molecular substrate matter? *Circ.: Arrhythmia Electrophysiol. 1*, 290−297.

(12) Kapa, S., Tester, D. J., Salisbury, B. A., Harris-Kerr, C., Pungliya, M. S., Alders, M., Wilde, A. A., and Ackerman, M. J. (2009) Genetic testing for long-QT syndrome: Distinguishing pathogenic mutations from benign variants. *Circulation 120*, 1752−1760.

(13) Jons, C., Moss, A. J., Lopes, C. M., McNitt, S., Zareba, W., Goldenberg, I., Qi, M., Wilde, A. A., Shimizu, W., Kanters, J. K., Towbin, J. A., Ackerman, M. J., and Robinson, J. L. (2009) Mutations in conserved amino acids in the KCNQ1 channel and risk of cardiac events in type-1 long-QT syndrome. *J. Cardiovasc. Electrophysiol. 20*, 859−865.

(14) Doyle, D. A., Morais Cabral, J., Pfuetzner, R. A., Kuo, A., Gulbis, J. M., Cohen, S. L., Chait, B. T., and MacKinnon, R. (1998) The structure of the potassium channel: Molecular basis of K^+ conduction and selectivity. *Science 280*, 69−77.

(15) Berneche, S., and Roux, B. (2001) Energetics of ion conduction through the K^+ channel. *Nature 414*, 73−77.

(16) Shrivastava, I. H., and Sansom, M. S. (2000) Simulations of ion permeation through a potassium channel: Molecular dynamics of KcsA in a phospholipid bilayer. *Biophys. J. 78*, 557−570.

(17) Berneche, S., and Roux, B. (2000) Molecular dynamics of the KcsA K^+ channel in a bilayer membrane. *Biophys. J. 78*, 2900−2917.

(18) Jensen, M. O., Borhani, D. W., Lindorff-Larsen, K., Maragakis, P., Jogini, V., Eastwood, M. P., Dror, R. O., and Shaw, D. E. (2010) Principles of conduction and hydrophobic gating in K^+ channels. *Proc. Natl. Acad. Sci. U.S.A. 107*, 5833−5838.

(19) Bastug, T., and Kuyucak, S. (2011) Comparative study of the energetics of ion permeation in Kv1.2 and KcsA potassium channels. *Biophys. J. 100*, 629−636.

(20) Berneche, S., and Roux, B. (2003) A microscopic view of ion conduction through the K^+ channel. *Proc. Natl. Acad. Sci. U.S.A. 100*, 8644−8648.

(21) Berneche, S., and Roux, B. (2005) A gate in the selectivity filter of potassium channels. *Structure 13*, 591−600.

(22) Bastug, T., and Kuyucak, S. (2009) Importance of the peptide backbone description in modeling the selectivity filter in potassium channels. *Biophys. J. 96*, 4006−4012.

(23) Choi, G., Kopplin, L. J., Tester, D. J., Will, M. L., Haglund, C. M., and Ackerman, M. J. (2004) Spectrum and frequency of cardiac channel defects in swimming-triggered arrhythmia syndromes. *Circulation 110*, 2119−2124.

(24) Napolitano, C., Priori, S. G., Schwartz, P. J., Bloise, R., Ronchetti, E., Nastoli, J., Bottelli, G., Cerrone, M., and Leonardi, S. (2005) Genetic testing in the long QT syndrome: Development and validation of an efficient approach to genotyping in clinical practice. *JAMA, J. Am. Med. Assoc. 294*, 2975−2980.

(25) Amin, A. S., Giudicessi, J. R., Tijsen, A. J., Spanjaart, A. M., Reckman, Y. J., Klemens, C. A., Tanck, M. W., Kapplinger, J. D., Hofman, N., Sinner, M. F., Muller, M., Wijnen, W. J., Tan, H. L., Bezzina, C. R., Creemers, E. E., Wilde, A. A., Ackerman, M. J., and Pinto, Y. M. (2012) Variants in the 3′ untranslated region of the KCNQ1-encoded Kv7.1 potassium channel modify disease severity in patients with type 1 long QT syndrome in an allele-specific manner. *Eur. Heart J. 33*, 714−723.

(26) Bartos, D. C., Duchatelet, S., Burgess, D. E., Klug, D., Denjoy, I., Peat, R., Lupoglazoff, J. M., Fressart, V., Berthet, M., Ackerman, M. J., January, C. T., Guicheney, P., and Delisle, B. P. (2011) R231C mutation in KCNQ1 causes long QT syndrome type 1 and familial atrial fibrillation. *Heart Rhythm 8*, 48−55.

(27) Zhou, Y., Morais-Cabral, J. H., Kaufman, A., and MacKinnon, R. (2001) Chemistry of ion coordination and hydration revealed by a K^+ channel-Fab complex at 2.0 Å resolution. *Nature 414*, 43−48.

(28) Humphrey, W., Dalke, A., and Schulten, K. (1996) VMD: Visual molecular dynamics. *J. Mol. Graphics 14*, 27−38.

(29) Phillips, J. C., Braun, R., Wang, W., Gumbart, J., Tajkhorshid, E., Villa, E., Chipot, C., Skeel, R. D., Kale, L., and Schulten, K. (2005) Scalable molecular dynamics with NAMD. *J. Comput. Chem. 26*, 1781−1802.

(30) Goldenberg, I., Moss, A. J., Peterson, D. R., McNitt, S., Zareba, W., Andrews, M. L., Robinson, J. L., Locati, E. H., Ackerman, M. J.,

Benhorin, J., Kaufman, E. S., Napolitano, C., Priori, S. G., Qi, M., Schwartz, P. J., Towbin, J. A., Vincent, G. M., and Zhang, L. (2008) Risk factors for aborted cardiac arrest and sudden cardiac death in children with the congenital long-QT syndrome. *Circulation 117*, 2184−2191.

(31) Hodgkin, A. L., and Keynes, R. D. (1955) The potassium permeability of a giant nerve fibre. *J. Physiol. 128*, 61−88.

(32) Ikrar, T., Hanawa, H., Watanabe, H., Aizawa, Y., Ramadan, M. M., Chinushi, M., and Horie, M. (2009) Evaluation of channel function after alteration of amino acid residues at the pore center of KCNQ1 channel. *Biochem. Biophys. Res. Commun. 378*, 589−594.

(33) Zareba, W., Moss, A. J., Sheu, G., Kaufman, E. S., Priori, S., Vincent, G. M., Towbin, J. A., Benhorin, J., Schwartz, P. J., Napolitano, C., Hall, W. J., Keating, M. T., Qi, M., Robinson, J. L., and Andrews, M. L. (2003) Location of mutation in the KCNQ1 and phenotypic presentation of long QT syndrome. *J. Cardiovasc. Electrophysiol. 14*, 1149−1153.

(34) Shimizu, W., Horie, M., Ohno, S., Takenaka, K., Yamaguchi, M., Shimizu, M., Washizuka, T., Aizawa, Y., Nakamura, K., Ohe, T., Aiba, T., Miyamoto, Y., Yoshimasa, Y., Towbin, J. A., Priori, S. G., and Kamakura, S. (2004) Mutation site-specific differences in arrhythmic risk and sensitivity to sympathetic stimulation in the LQT1 form of congenital long QT syndrome: multicenter study in Japan. *J. Am. Coll. Cardiol. 44*, 117−125.

(35) Moss, A. J., Shimizu, W., Wilde, A. A., Towbin, J. A., Zareba, W., Robinson, J. L., Qi, M., Vincent, G. M., Ackerman, M. J., Kaufman, E. S., Hofman, N., Seth, R., Kamakura, S., Miyamoto, Y., Goldenberg, I., Andrews, M. L., and McNitt, S. (2007) Clinical aspects of type-1 long-QT syndrome by location, coding type, and biophysical function of mutations involving the KCNQ1 gene. *Circulation 115*, 2481−2489.

(36) Smith, J. A., Vanoye, C. G., George, A. L., Jr., Meiler, J., and Sanders, C. R. (2007) Structural models for the KCNQ1 voltage-gated potassium channel. *Biochemistry 46*, 14141−14152.

(37) Strutz-Seebohm, N., Pusch, M., Wolf, S., Stoll, R., Tapken, D., Gerwert, K., Attali, B., and Seebohm, G. (2011) Structural basis of slow activation gating in the cardiac I Ks channel complex. *Cell. Physiol. Biochem. 27*, 443−452.

(38) Barhanin, J., Lesage, F., Guillemare, E., Fink, M., Lazdunski, M., and Romey, G. (1996) K(V)LQT1 and lsK (minK) proteins associate to form the I(Ks) cardiac potassium current. *Nature 384*, 78−80.

(39) Sanguinetti, M. C., Curran, M. E., Zou, A., Shen, J., Spector, P. S., Atkinson, D. L., and Keating, M. T. (1996) Coassembly of K(V)LQT1 and minK (IsK) proteins to form cardiac I(Ks) potassium channel. *Nature 384*, 80−83.

(40) Panaghie, G., Tai, K. K., and Abbott, G. W. (2006) Interaction of KCNE subunits with the KCNQ1 K^+ channel pore. *J. Physiol. 570*, 455−467.

(41) Panaghie, G., Purtell, K., Tai, K. K., and Abbott, G. W. (2008) Voltage-dependent C-type inactivation in a constitutively open K^+ channel. *Biophys. J. 95*, 2759−2778.

(42) McCoy, J. G., and Nimigean, C. M. (2012) Structural correlates of selectivity and inactivation in potassium channels. *Biochim. Biophys. Acta 1818*, 272−285.

(43) Cuello, L. G., Jogini, V., Cortes, D. M., Pan, A. C., Gagnon, D. G., Dalmas, O., Cordero-Morales, J. F., Chakrapani, S., Roux, B., and Perozo, E. (2010) Structural basis for the coupling between activation and inactivation gates in K^+ channels. *Nature 466*, 272−275.

(44) Cuello, L. G., Jogini, V., Cortes, D. M., and Perozo, E. (2010) Structural mechanism of C-type inactivation in K^+ channels. *Nature 466*, 203−208.